

MIT Open Access Articles

The R-Process Alliance: a comprehensive abundance analysis of HD 222925, a metal-poor star with an extreme R-process enhancement of $[Eu/H] = -0.14^$*

The MIT Faculty has made this article openly available. **Please share** how this access benefits you. Your story matters.

Citation: Roederer, Ian U., et al., "The R-Process Alliance: a comprehensive abundance analysis of HD 222925, a metal-poor star with an extreme R-process enhancement of $[Eu/H] = -0.14^*$." *Astrophysical journal* 865, 2 (October 2018): no. 129 doi 10.3847/1538-4357/AADD92 ©2018 Author(s)

As Published: 10.3847/1538-4357/AADD92

Publisher: American Astronomical Society

Persistent URL: <https://hdl.handle.net/1721.1/124740>








Version: Final published version: final published article, as it appeared in a journal, conference proceedings, or other formally published context

Terms of Use: Article is made available in accordance with the publisher's policy and may be subject to US copyright law. Please refer to the publisher's site for terms of use.





The *R*-Process Alliance: A Comprehensive Abundance Analysis of HD 222925, a Metal-poor Star with an Extreme *R*-process Enhancement of $[\text{Eu}/\text{H}] = -0.14^*$

Ian U. Roederer^{1,2} , Charli M. Sakari³ , Vinicius M. Placco^{2,4} , Timothy C. Beers^{2,4} , Rana Ezzeddine^{2,5} ,
Anna Frebel^{2,5} , and Terese T. Hansen⁶ 

¹Department of Astronomy, University of Michigan, 1085 S. University Ave., Ann Arbor, MI 48109, USA; iur@umich.edu

²Joint Institute for Nuclear Astrophysics—Center for the Evolution of the Elements (JINA-CEE), USA

³Department of Astronomy, University of Washington, Seattle, WA 98195-1580, USA

⁴Department of Physics, University of Notre Dame, Notre Dame, IN 46556, USA

⁵Department of Physics and Kavli Institute for Astrophysics and Space Research, Massachusetts Institute of Technology, Cambridge, MA 02139, USA

⁶Carnegie Observatories, Pasadena, CA 91101, USA

Received 2018 July 31; revised 2018 August 24; accepted 2018 August 25; published 2018 October 1

Abstract

We present a detailed abundance analysis of the bright ($V = 9.02$), metal-poor ($[\text{Fe}/\text{H}] = -1.47 \pm 0.08$) field red horizontal-branch star HD 222925, which was observed as part of an ongoing survey by the *R*-Process Alliance. We calculate stellar parameters and derive abundances for 46 elements based on 901 lines examined in a high-resolution optical spectrum obtained using the Magellan Inamori Kyocera Echelle spectrograph. We detect 28 elements with $38 \leq Z \leq 90$; their abundance pattern is a close match to the solar *r*-process component. The distinguishing characteristic of HD 222925 is an extreme enhancement of *r*-process elements ($[\text{Eu}/\text{Fe}] = +1.33 \pm 0.08$, $[\text{Ba}/\text{Eu}] = -0.78 \pm 0.10$) in a moderately metal-poor star, so the abundance of *r*-process elements is the highest ($[\text{Eu}/\text{H}] = -0.14 \pm 0.09$) in any known *r*-process-enhanced star. The abundance ratios among lighter ($Z \leq 30$) elements are typical for metal-poor stars, indicating that production of these elements was dominated by normal Type II supernovae, with no discernible contributions from Type Ia supernovae or asymptotic giant branch stars. The chemical and kinematic properties of HD 222925 suggest it formed in a low-mass dwarf galaxy, which was enriched by a high-yield *r*-process event before being disrupted by interaction with the Milky Way.

Key words: nuclear reactions, nucleosynthesis, abundances – stars: abundances – stars: individual (HD 222925)

Supporting material: machine-readable table

1. Introduction

The rapid neutron-capture process, or *r*-process, is one of the fundamental ways to produce the heaviest elements found in nature. Decades of theoretical and observational efforts to understand and characterize the *r*-process are summarized in reviews by Qian & Wasserburg (2007), Sneden et al. (2008), Thielemann et al. (2017), Frebel (2018), and Horowitz et al. (2018). Recent analysis of the “kilonova” electromagnetic counterpart (e.g., Cowperthwaite et al. 2017; Drout et al. 2017; Kasen et al. 2017; Tanvir et al. 2017) to a merger of two neutron stars detected in gravitational waves (GW170817; Abbott et al. 2017a, 2017b) confirms earlier observational suggestions (e.g., Beniamini et al. 2016; Ji et al. 2016a) that neutron star mergers are viable *r*-process sites. No individual lines of *r*-process elements can be confidently identified in the kilonova spectra, but hundreds of such lines are regularly detected in spectra of highly *r*-process-enhanced stars in the Milky Way. The existence, abundance patterns, and occurrence frequencies of these stars have established that the abundance pattern produced by the *r*-process has remained largely unchanged across 9 Gyr of cosmic time before the Sun was formed.

Highly *r*-process-enhanced stars have minimal contamination from the slow neutron-capture process (*s*-process), as well as Eu/Fe ratios >10 times higher than found in the Sun (expressed as $[\text{Eu}/\text{Fe}] > +1.0$, where the abundance ratio of

Eu and Fe relative to the solar ratio, $[\text{Eu}/\text{Fe}]$, is defined as $\log_{10}(N_{\text{Eu}}/N_{\text{Fe}}) - \log_{10}(N_{\text{Eu}}/N_{\text{Fe}})_{\odot}$). These stars are often referred to as *r*-II stars (Beers & Christlieb 2005). The abundance of the element Eu ($Z = 63$) is commonly used to represent the level of *r*-process enhancement. CS 22892-052, which has $[\text{Eu}/\text{Fe}] = +1.6$, was the first recognized *r*-II star (Sneden et al. 1994). This star was identified in the HK Survey of Beers et al. (1992). Since then, the average rate of discovery of *r*-II stars has been $\lesssim 1 \text{ yr}^{-1}$. The low discovery rate reflects the rarity of these stars. The occurrence frequency of *r*-II stars is $\approx 3\%$ among stars with $[\text{Fe}/\text{H}] < -1.5$ (Barklem et al. 2005), which themselves only constitute $\lesssim 1\%$ of all stars in the solar neighborhood.

Expanding the sample of confirmed *r*-process-enhanced stars is one of the goals of a new effort called the *R*-Process Alliance (RPA). The first large samples analyzed by the RPA have been presented by Hansen et al. (2018) and Sakari et al. (2018a), and new discoveries of individual *r*-process-enhanced stars have been presented by Placco et al. (2017), Cain et al. (2018), Gull et al. (2018), Holmbeck et al. (2018a), and Sakari et al. (2018b). Most RPA candidates have been selected from the RAdial Velocity Experiment (Kordopatis et al. 2013; Kunder et al. 2017), the LAMOST Survey (Liu et al. 2014), and the Best & Brightest Survey (Schlaufman & Casey 2014). Here, we present a new *r*-II star, HD 222925. We identified HD 222925 as a candidate for our observing program by browsing the literature of the last few decades in search of bright, metal-poor F- or G-type stars with insufficiently characterized heavy-element abundance patterns.

* This paper includes data gathered with the 6.5 m Magellan Telescopes located at Las Campanas Observatory, Chile.

Table 1
Basic Data for HD 222925

Quantity	Symbol	Value	Units	References
R.A.	α (J2000)	23:45:17.61	hh:mm:ss.ss	Simbad
Decl.	δ (J2000)	-61:54:42.8	dd:mm:ss.s	Simbad
Galactic longitude	l	316.0	degrees	Simbad
Galactic latitude	b	-53.5	degrees	Simbad
Parallax	ϖ	2.2332 ± 0.0243	mas	Lindgren et al. (2018)
Inverse parallax distance	$1/\varpi$	448 ± 5	pc	This study
Distance	D	$442_{-4.7}^{+4.9}$	pc	Bailer-Jones et al. (2018)
Proper motion (α)	PMRA	154.854 ± 0.041	mas yr ⁻¹	Lindgren et al. (2018)
Proper motion (δ)	PMDec	-99.171 ± 0.041	mas yr ⁻¹	Lindgren et al. (2018)
Radial velocity	RV	-38.9 ± 0.6	km s ⁻¹	This study
Mass	Mass	0.75 ± 0.20	M_{\odot}	Assumed
B magnitude	B	9.61 ± 0.02	mag	Norris et al. (1985)
V magnitude	V	9.02 ± 0.02	mag	Norris et al. (1985)
J magnitude	J	7.747 ± 0.023	mag	Cutri et al. (2003)
H magnitude	H	7.415 ± 0.029	mag	Cutri et al. (2003)
K magnitude	K	7.338 ± 0.026	mag	Cutri et al. (2003)
Color excess	$E(B - V)$	$0.00_{-0.00}^{+0.02}$	mag	This study
Bolometric correction	BC_V	-0.21 ± 0.07	mag	Based on Casagrande & Vandenberg (2014)
Effective temperature	T_{eff}	5636 ± 103	K	This study
Log of surface gravity	$\log g$	2.54 ± 0.17	(cgs)	This study
Microturbulent velocity	v_t	2.20 ± 0.20	km s ⁻¹	This study
Model metallicity	[M/H]	-1.5 ± 0.1	dex	This study
Metallicity	[Fe/H]	-1.47 ± 0.08	dex	This study

Table 1 lists the basic properties of HD 222925. Houk & Cowley (1975) classified it as a chemically peculiar “Sr Eu” star. The abundances of metals in the atmosphere of HD 222925 reflect their bulk abundances in the star, so it is not chemically peculiar in the traditional sense. Houk & Cowley were, however, the first to recognize the presence of strong second spectra lines (i.e., lines arising from electronic transitions of ionized species) in HD 222925.

Two modern studies have analyzed limited sets of elements in HD 222925. Gratton et al. (2000) analyzed the pattern of light element abundance variations for 62 metal-poor stars at various stages of stellar evolution. They identified HD 222925 as a field equivalent of the cluster red horizontal-branch (RHB) stars, deriving an effective temperature (T_{eff}) of 5564 K, surface gravity ($\log g$) of 2.64, and metallicity ([Fe/H]) of -1.51 . Navarrete et al. (2015) used HD 222925 as part of a control sample of field stars in their abundance study that found no association between tidal stellar debris from ω Cen and the Kapteyn moving group. Navarrete et al. derived $T_{\text{eff}} = 5710 \pm 60$ K, $\log g = 2.32 \pm 0.14$, and $[\text{Fe}/\text{H}] = -1.37 \pm 0.05$. Their study found that the He I line at 10830 Å in HD 222925 was several times stronger than that in other metal-poor field stars, which they speculated could be due to chromospheric activity. The three RHB stars in their study have the strongest He I lines, so we presume that the line strength is related to the evolutionary state and not a natal enhancement of He. Their study was also the first to quantify the enhanced level of Ba in HD 222925, $[\text{Ba}/\text{Fe}] = +0.85 \pm 0.20$, but they did not consider any elements heavier than Ba. Navarrete et al. suggested the enhanced Ba could result from mass transfer of s -process rich material from an unseen companion star that passed through the asymptotic giant branch (AGB) phase of evolution. They proposed to test this hypothesis by searching for radial velocity (RV) variations or Y or Tc abundances, but they did not pursue the matter further.

We present a comprehensive abundance analysis of HD 222925 based on new high-resolution optical spectroscopy. Throughout this work, we adopt the standard nomenclature for elemental abundances and ratios. The absolute abundance of an element X is defined as the number of X atoms per 10^{12} H atoms, $\log \varepsilon(\text{X}) \equiv \log_{10}(N_{\text{X}}/N_{\text{H}}) + 12.0$. We adopt the solar photospheric abundances of Asplund et al. (2009). By convention, abundances or ratios denoted with the ionization state are understood to be the total elemental abundance, as derived from transitions of that particular ionization state after Saha ionization corrections have been applied.

2. Observations

We observed HD 222925 on 2017 September 26 using the Magellan Inamori Kyocera Echelle spectrograph (MIKE; Bernstein et al. 2003) mounted at the $f/11$ focus on the east Nasmyth platform of the Landon Clay (Magellan II) Telescope at Las Campanas Observatory, Chile. A pair of 50 s observations of HD 222925 using the $0''.7 \times 5''.0$ entrance slit and 2×2 binning revealed a strong Eu II absorption line at 3819 Å. Preliminary analyses over the subsequent 48 hr indicated super-solar [Eu/La] and [Eu/Ba] ratios, suggesting that the heavy-element enhancement might be dominated by r -process nucleosynthesis.

We reobserved HD 222925 with MIKE on 2017 September 28 with a series of 300 and 600 s exposures, totaling 115 minutes. These observations used the $0''.35 \times 5''.0$ entrance slit and the native 1×1 detector binning. This setup yielded a spectral resolving power $R \equiv \lambda/\Delta\lambda \sim 68,000$ on the blue spectrograph ($\lambda \lesssim 5000$ Å) and $R \sim 61,000$ on the red spectrograph, as measured from isolated emission lines in the comparison lamp spectra. The outside temperature was changing somewhat during the observations, and the instrument was slightly out of focus, so the resolving power is lower than could otherwise be achieved with this observing setup.

The observations were made with HD 222925 at an airmass between 1.19 and 1.22. The seeing ranged from $0''.6$ to $1''.0$ arcsec, and thin but variable clouds were present throughout these observations. We also observed a bright, rapidly rotating B3V star, HIP 98412, to divide out telluric lines from our spectra, and a comparison metal-poor field RHB star, HD 184266, with the same MIKE setup.

We use the CarPy MIKE reduction pipeline (Kelson et al. 2000; Kelson 2003) as the primary data reduction method. This includes overscan subtraction, pixel-to-pixel flat field division, image coaddition, cosmic-ray removal, sky and scattered-light subtraction, rectification of the tilted slit profiles along the orders, spectrum extraction, and wavelength calibration. We modify some of the default pipeline settings to work on data binned 1×1 with the $0''.35 \times 5''.0$ slit, yet the wavelength solution produced by the pipeline is unsatisfactory for the bluest 18 orders of our data. For these, we manually generate the wavelength solution using routines in the IRAF “echelle” package. We also use IRAF to stitch together the individual orders, continuum-normalize the spectra, and shift the spectra to rest velocity.

Our final spectrum of HD 222925 covers $3330 < \lambda < 9410 \text{ \AA}$, although the spectra longward of $\sim 8000 \text{ \AA}$ show evidence of fringing. Signal-to-noise ratios (S/N) in the continuum range from $\sim 80/1 \text{ pix}^{-1}$ near 3400 \AA , $\sim 250/1 \text{ pix}^{-1}$ near 4000 \AA , $\sim 500/1 \text{ pix}^{-1}$ near 4550 \AA , and $\sim 500/1 \text{ pix}^{-1}$ near 5200 \AA , to $\sim 700/1 \text{ pix}^{-1}$ near 6750 \AA . HD 222925 has fairly broad absorption lines (median $\approx 6.5 \text{ km s}^{-1}$ for the Fe lines measured in Section 3.1), which is typical for RHB stars. This results in fewer completely unblended lines, but each line is greatly oversampled by ≈ 20 – 30 pixels, or ~ 8 resolution elements, in our spectrum. The predicted 3σ line detection thresholds (Cayrel 1988; Frebel et al. 2008) for these data are $\approx 1 \text{ m\AA}$.

2.1. Radial Velocity

We measure the RV of HD 222925 by cross-correlating the order containing the Mg I *b* triplet against a metal-poor template (HD 128279) observed with MIKE (Roederer et al. 2014b). We calculate the Heliocentric correction using the IRAF “rvcorrect” task. Our measured heliocentric RV, $-38.9 \pm 0.6 \text{ km s}^{-1}$, agrees with that measured by Navarrete et al. (2015), $-38.64 \pm 0.36 \text{ km s}^{-1}$, and the RV reported by the second data release (DR2) of the *Gaia* mission (Katz et al. 2018; Lindegren et al. 2018), $-37.93 \pm 0.28 \text{ km s}^{-1}$. Beers et al. (2014) measured an RV of $-34 \pm 7 \text{ km s}^{-1}$ from medium-resolution ($R \sim 3000$) spectroscopy, which is consistent with these values. Thus, HD 222925 shows no evidence of RV variations that would signal the presence of an unseen companion.

3. Stellar Parameters

3.1. Fe Lines

We compile a list of Fe I lines with reliable oscillator strengths from the National Institute of Standards and Technology (NIST) Atomic Spectral Database (ASD) (Kramida et al. 2018) with grades B or better ($\leq 10\%$ uncertainty, or 0.05 dex). These $\log gf$ values mainly come from work by O’Brian et al. (1991). We supplement this list with results from recent laboratory studies with comparable uncertainties (Den Hartog et al. 2014; Ruffoni et al. 2014; Belmonte et al. 2017). We discard Fe I lines with lower

excitation potential (E.P.) $< 1.2 \text{ eV}$, because previous studies have shown that these lines may yield higher-than-average abundances in metal-poor dwarfs and giants (e.g., Cayrel et al. 2004; Cohen et al. 2008) likely caused by departures from local thermodynamic equilibrium (LTE) (e.g., Bergemann et al. 2012). We also adopt $\log gf$ values for Fe II lines from NIST, retaining lines with grades C or better ($\leq 25\%$ uncertainty, 0.12 dex).

We measure equivalent widths (EWs) using a semi-automatic routine that fits Voigt or Gaussian line profiles to continuum-normalized spectra (Roederer et al. 2014a). We visually inspect each line, and we discard from consideration any line that appears blended, is subject to uncertain continuum placement, or is otherwise compromised. We examine a telluric spectrum simultaneously with the stellar spectrum, and any lines that appear to be contaminated with telluric absorption are also discarded. We restrict ourselves to lines with $\log(\text{EW}/\lambda) < -4.5$. We retain 124 Fe I lines and 10 Fe II lines, whose EWs are reported in Table 2.

3.2. Model Atmosphere Parameters

Table 1 summarizes the broadband photometry we have compiled for HD 222925. The Schlafly & Finkbeiner (2011) dust maps predict that the total Galactic reddening along the line of sight to HD 222925 is small, $E(B - V) = 0.019$. We independently check the reddening by inspecting our spectrum for evidence of interstellar absorption near the Na I doublet at 5889 and 5895 \AA . We use the IRAF “telluric” task to remove telluric lines from this region of the spectrum of HD 222925 by comparing with our hot star standard. No interstellar Na I absorption is detected toward HD 222925, so we adopt $E(B - V) = 0.00_{-0.00}^{+0.02}$. We deredden using the extinction coefficients of McCall (2004).

We calculate T_{eff} from the metallicity-dependent color- T_{eff} relations presented by Casagrande et al. (2010). The zeropoint of this scale was determined using solar twins, and Casagrande et al. (2014) showed that it is also applicable to giants. We adopt a metallicity of $[\text{Fe}/\text{H}] = -1.5 \pm 0.3$ based on previous work (Gratton et al. 2000; Navarrete et al. 2015). We draw 10^4 samples from each input parameter (magnitudes, reddening, and metallicity) and calculate the T_{eff} value predicted by each one. Each calculation is self-consistent and uses the same set of input draws, and we adopt the median of the final distribution as T_{eff} . Five colors ($B - V$, $V - J$, $V - H$, $V - K$, $J - K$) yield consistent estimates of $5644 \pm 133 \text{ K}$, $5628 \pm 74 \text{ K}$, $5641 \pm 64 \text{ K}$, $5630 \pm 54 \text{ K}$, and $5714 \pm 215 \text{ K}$, respectively. The weighted average and statistical uncertainty in T_{eff} is $5636 \pm 46 \text{ K}$. We estimate the systematic uncertainty by performing the same set of calculations for two other color- T_{eff} calibrations presented by Alonso et al. (1999) and Ramírez & Meléndez (2005). These scales predict $5505 \pm 72 \text{ K}$ and $5458 \pm 38 \text{ K}$, respectively. We adopt the quadrature sum of the statistical uncertainty from Casagrande et al. (2010) (46 K) and the standard deviation of these three T_{eff} values (92 K) as the total uncertainty on T_{eff} (103 K).

We calculate the $\log g$ value from fundamental relations:

$$\log g = 4 \log T_{\text{eff}} + \log(M/M_{\odot}) - 10.61 + 0.4(\text{BC}_V + V + 5 \log \varpi + 5 - 3.1E(B - V) - M_{\text{bol},\odot}). \quad (1)$$

The symbols and their values are given in Table 1. $M_{\text{bol},\odot}$ is the solar bolometric magnitude, 4.75, and the constant 10.61 is

Table 2
Lines, Atomic Data, EWs, and Abundances

Species	Wavelength (Å)	E.P. (eV)	$\log gf$	$\log gf$ ref.	EW (mÅ)	Limit Flag	$\log \epsilon$
Li I	6707.80	0.00	0.17	1	...	<	0.800
Na I	4982.81	2.10	-0.92	2	2.8	...	4.286
Na I	5682.63	2.10	-0.71	2	10.5	...	4.581

References. (1) Smith et al. (1998), using HFS/IS from Kurucz & Bell (1995); (2) Kramida et al. (2018); (3) Pehlivan Rhodin et al. (2017); (4) Aldenius et al. (2009); (5) Lawler & Dakin (1989), using HFS from Kurucz & Bell (1995); (6) Lawler et al. (2013); (7) Wood et al. (2013); (8) Lawler et al. (2014) for $\log gf$ values and HFS; (9) Wood et al. (2014a) for $\log gf$ values and HFS, when available; (10) Sobek et al. (2007); (11) Lawler et al. (2017); (12) Den Hartog et al. (2011) for $\log gf$ values and HFS; (13) O’Brian et al. (1991); (14) Den Hartog et al. (2014); (15) Belmonte et al. (2017); (16) Ruffoni et al. (2014); (17) Lawler et al. (2015) for $\log gf$ values and HFS; (18) Wood et al. (2014b); (19) Kramida et al. (2018), using HFS/IS from Kurucz & Bell (1995); (20) Roederer & Lawler (2012); (21) Morton (2000); (22) Biémont et al. (2011); (23) Ljung et al. (2006); (24) Nilsson & Ivarsson (2008); (25) Wickliffe et al. (1994); (26) Duquette & Lawler (1985); (27) Hansen et al. (2012) for $\log gf$ value and HFS/IS; (28) Kramida et al. (2018), using HFS/IS from McWilliam (1998) when available; (29) Lawler et al. (2001a), using HFS from Ivans et al. (2006) when available; (30) Lawler et al. (2009); (31) Li et al. (2007), using HFS from Sneden et al. (2009); (32) Ivarsson et al. (2001), using HFS from Sneden et al. (2009); (33) Den Hartog et al. (2003), using HFS/IS from Roederer et al. (2008) when available; (34) Lawler et al. (2006), using HFS/IS from Roederer et al. (2008) when available; (35) Lawler et al. (2001c), using HFS/IS from Ivans et al. (2006); (36) Den Hartog et al. (2006); (37) Lawler et al. (2001b), using HFS from Lawler et al. (2001d); (38) Wickliffe et al. (2000); (39) Lawler et al. (2004), using HFS from Sneden et al. (2009); (40) Lawler et al. (2008); (41) Wickliffe & Lawler (1997), using HFS from Sneden et al. (2009); (42) Sneden et al. (2009) for $\log gf$ value and HFS/IS; (43) Lawler et al. (2009) for $\log gf$ values and HFS; (44) Lawler et al. (2007); (45) Quinet et al. (2006); (46) Xu et al. (2007), using HFS/IS from Cowan et al. (2005); (47) Biémont et al. (2000), using HFS/IS from Roederer et al. (2012); (48) Nilsson et al. (2002b); (49) Nilsson et al. (2002a).

(This table is available in its entirety in machine-readable form.)

calculated from the solar constants $\log T_{\text{eff}\odot} = 3.7617$ and $\log g_{\odot} = 4.438$. We draw 10^4 samples from each of these input parameters. The median of these calculations gives the $\log g$ value, and their standard deviation gives the uncertainty: 2.54 ± 0.17 . The T_{eff} and $\log g$ values we calculate for HD 222925 are in good agreement with those determined by Gratton et al. (2000) and Navarrete et al. (2015), quoted in Section 1. They are also consistent with the values derived from high-S/N medium-resolution spectroscopy by Beers et al. (2014): $T_{\text{eff}} = 5603 \pm 125$ K and $\log g = 2.2 \pm 0.4$.

We interpolate a one-dimensional, hydrostatic model atmosphere from the α -enhanced ATLAS9 grid of models (Castelli & Kurucz 2004), using an interpolation code provided by A. McWilliam (2009, private communication). We derive Fe abundances using a recent version of the line analysis software MOOG (Sneden 1973; 2017 version). MOOG assumes that LTE holds in the line-forming layers of the atmosphere. This version of the code treats Rayleigh scattering—which affects the continuous opacity at shorter wavelengths—as isotropic, coherent scattering, as described in Sobek et al. (2011). We adopt damping constants for collisional broadening with neutral hydrogen from Barklem et al. (2000) and Barklem & Aspelund-Johansson (2005), when available; otherwise, we adopt the standard Unsold (1955) recipe.

We iteratively determine the microturbulent velocity, v_t , and model metallicity, $[M/H]$. Lines yielding an abundance more than 0.4 dex from the mean are culled. Convergence is reached when there is no dependence between line strength and abundance derived from Fe I lines, and when $[M/H]$ equals the average of the abundances derived from Fe I and Fe II lines, rounded to the nearest 0.1 dex. We find $v_t = 2.20 \pm 0.2$ km s $^{-1}$ and $[M/H] = -1.5 \pm 0.1$ dex. Our adopted model atmosphere parameters for HD 222925 are listed in Table 1.

We compute $[\text{Fe I}/\text{H}]$ and $[\text{Fe II}/\text{H}]$ ratios, and their difference, by drawing 10^3 samples from each input parameter in the model atmosphere (T_{eff} , $\log g$, v_t , and $[M/H]$) from normal distributions. We interpolate a new model atmosphere

for each of these draws, and the abundances are recomputed for each line. We associate an EW uncertainty with each line, given by $\sqrt{(0.05 \times \text{EW})^2 + 1.0}$, which asymptotes to 1 mÅ for the weakest lines and 5% for the strongest lines. We sample the $\log gf$ value for each line from a normal distribution whose dispersion is given by the $\log gf$ uncertainty (see references to Table 2). We adopt the median of these 10^3 realizations as the average Fe abundance. The 16th and 84th percentiles of the distributions are roughly symmetric, so we report one number as the systematic uncertainty, σ . These values are reported in Table 3.

We find only a small offset between the Fe abundances derived from Fe I and Fe II lines: $[\text{Fe I}/\text{H}] = -1.58 \pm 0.01$ ($\sigma = 0.08$ dex) and $[\text{Fe II}/\text{H}] = -1.47 \pm 0.03$ ($\sigma = 0.08$ dex). Their difference, $[\text{Fe II}/\text{H}] - [\text{Fe I}/\text{H}] = +0.11 \pm 0.03$ dex ($\sigma = 0.10$ dex), is small but significant. This suggests that transitions in neutral Fe may not be adequately characterized by Boltzmann and Saha LTE calculations, even when low-E.P. Fe I lines and strong lines are excluded from consideration. Non-LTE over-ionization may be responsible. Singly ionized Fe atoms are expected to dominate (>98%) by number in the line-forming layers of HD 222925, so LTE is an acceptable approximation for Fe II lines. We confirm this hypothesis by interpolating non-LTE corrections for 14 Fe I lines in common with the INSPECT database (Bergemann et al. 2012; Lind et al. 2012). Their average non-LTE correction is +0.12 dex, which would bring the $[\text{Fe}/\text{H}]$ ratio derived from Fe I lines into good agreement with that derived from Fe II lines. Extrapolating the simple linear relation between $[\text{Fe}/\text{H}]$ and the non-LTE correction to abundances derived from Fe I lines found by Ezzeddine et al. (2017) predicts a similar correction of +0.07 dex. We conclude that departures from LTE are likely responsible for the discrepancy between the $[\text{Fe}/\text{H}]$ ratios derived from Fe I and II lines in HD 222925.

4. Visual Inspection of the Spectrum of HD 222925

Figure 1 illustrates three small regions of the spectrum of HD 222925. Another RHB star with similar stellar parameters,

Table 3
Derived Abundances

Species	$\log \varepsilon$	σ	[X/Fe] ^a	σ	N_{lines}
Fe I	5.92	0.08	-1.58	0.08	124
Fe II	6.03	0.08	-1.47	0.08	10
Li I	<0.80	1
C (CH)	6.65	0.15	-0.20	0.17	...
N (NH)	6.45	0.20	+0.20	0.21	...
Na I	4.49	0.07	-0.17	0.07	7
Mg I	6.43	0.08	+0.41	0.05	7
Al I	4.80	0.17	-0.07	0.17	3
Si I	6.38	0.07	+0.45	0.07	18
K I	3.68	0.10	+0.23	0.04	1
Ca I	5.12	0.08	+0.36	0.05	34
Sc II	1.82	0.13	+0.14	0.08	8
Ti I	3.60	0.11	+0.23	0.03	13
Ti II	3.88	0.09	+0.40	0.05	14
V I	2.38	0.11	+0.03	0.04	3
V II	2.65	0.11	+0.19	0.08	12
Cr I	3.95	0.11	-0.11	0.03	15
Cr II	4.16	0.08	-0.01	0.05	6
Mn I	3.55	0.08	-0.30	0.02	13
Mn II	3.78	0.19	-0.18	0.16	3
Co I	3.33	0.18	-0.08	0.10	21
Ni I	4.62	0.09	-0.02	0.02	13
Cu I	2.05	0.15	-0.56	0.12	1
Zn I	3.17	0.06	+0.19	0.04	3
Rb I	<2.10	...	<+1.16	...	2
Sr I	1.46	0.11	+0.17	0.05	1
Sr II	1.98	0.13	+0.58	0.13	3
Y II	1.04	0.10	+0.30	0.07	40
Zr II	1.74	0.10	+0.63	0.07	51
Nb II	0.61	0.16	+0.62	0.15	1
Mo I	1.30	0.15	+1.00	0.09	3
Ru I	1.34	0.14	+1.17	0.08	5
Rh I	0.64	0.16	+1.31	0.12	3
Pd I	1.05	0.15	+1.06	0.08	3
Ag I	0.44	0.18	+1.08	0.13	1
Ba II	1.26	0.09	+0.55	0.06	5
La II	0.51	0.09	+0.88	0.07	40
Ce II	0.85	0.08	+0.74	0.07	67
Pr II	0.22	0.10	+0.97	0.08	22
Nd II	0.88	0.09	+0.93	0.08	99
Sm II	0.62	0.09	+1.13	0.08	87
Eu II	0.38	0.09	+1.33	0.08	17
Gd II	0.82	0.09	+1.22	0.08	38
Tb II	0.16	0.10	+1.33	0.08	3
Dy II	1.01	0.11	+1.38	0.08	32
Ho II	0.12	0.15	+1.11	0.12	9
Er II	0.74	0.10	+1.29	0.08	13
Tm II	-0.13	0.10	+1.24	0.08	7
Yb II	0.48	0.18	+1.11	0.17	1
Lu II	0.06	0.13	+1.43	0.09	2
Hf II	0.37	0.09	+0.99	0.09	5
Os I	1.26	0.15	+1.44	0.09	2
Ir I	1.54	0.16	+1.74	0.11	1
Pb I	<1.10	...	<+0.93	...	1
Th II	-0.06	0.12	+1.39	0.11	5
U II	<-0.50	...	<+1.51	...	2

Note.^a [Fe/H] values listed for Fe I and Fe II.

HD 184266, is shown for comparison in Figure 1. We rederive the stellar parameters for HD 184266 using the methods described in Section 3.2. We find $T_{\text{eff}} = 5580 \pm$

102 K, $\log g = 2.50 \pm 0.19$, $v_t = 2.25 \pm 0.20 \text{ km s}^{-1}$, and $[\text{Fe I}/\text{H}] = -1.80 \pm 0.08$, which are similar to the values we find for HD 222925, $T_{\text{eff}} = 5636 \pm 103 \text{ K}$, $\log g = 2.54 \pm 0.17$, $v_t = 2.20 \pm 0.20 \text{ km s}^{-1}$, and $[\text{Fe I}/\text{H}] = -1.58 \pm 0.08$. It is apparent from Figure 1 that the lines of Fe-group species in HD 184266 are slightly weaker than those in HD 222925, and our analysis confirms that the metallicity of HD 184266 is slightly lower. The contrast between the two stars is most apparent in the strengths of absorption lines from heavy ($Z > 30$) elements, which are indicated in red. Many of these lines are weak or absent in the spectrum of HD 184266, but they are strong in the spectrum of HD 222925.

Figure 1 also demonstrates how incredibly rich the spectrum of HD 222925 is with lines of heavy elements. Fourteen species of heavy elements are detectable in these three spectral windows. The other remarkable characteristic of the spectrum of HD 222925 is the contrast between the lines of Fe-group elements and heavy elements. The abundance of Eu atoms in HD 222925 is 72% of that in the Sun ($[\text{Eu}/\text{H}] = -0.14$; calculated from data in Table 3), yet the abundance of Fe atoms in HD 222925 is only 3% of that in the Sun ($[\text{Fe}/\text{H}] = -1.47$). The warm, low-pressure atmosphere of HD 222925 further minimizes blends from lines of neutral Fe-group elements while enhancing lines of ionized n -capture elements.

5. Abundance Analysis

We use the MOOG “abfind” driver to derive abundances of most elements with $Z \leq 30$ based on EW measurements. These values are reported in Table 2. Lines of Sc II, V I and II, Mn I and II, Co I,⁷ and Cu I are broadened by hyperfine splitting structure (HFS), so we derive their abundances by spectrum synthesis matching using the MOOG “synth” driver. All elements heavier than Zn are also derived by spectrum synthesis matching. We also derive an upper limit on the Li, Rb, Pb, and U abundances using spectrum synthesis matching. We derive abundances or upper limits from 901 lines in the spectrum on HD 222925, including 571 lines of elements with $Z > 30$. Table 2 lists the wavelengths of these lines, their E.P. values, $\log gf$ values, references for the $\log gf$ values and any HFS or isotope shifts (IS) considered in the syntheses, and the derived abundances. Multiple isotopes are considered in the synthesis for Li, C, Cu, Ag, Ba, Nd, Sm, Eu, Yb, Ir, and Pb. We adopt ${}^7\text{Li}/{}^6\text{Li} = 1000$, ${}^{12}\text{C}/{}^{13}\text{C} = 5$ (see below), ${}^{63}\text{Cu}/{}^{65}\text{Cu} = 2.24$ (the solar ratio), and the r -process isotopic fractions from Sneden et al. (2008) for all other elements.

We derive C and N abundances by iteratively fitting portions of the CH G -band (4290–4315 Å) and the NH band (3355–3365 Å). We estimate $[\text{C}/\text{Fe}] = -0.20 \pm 0.17$ and $[\text{N}/\text{Fe}] = +0.20 \pm 0.21$, giving $\text{C}/\text{N} = 1.6$. These molecular features are relatively weak in the spectrum, and no ${}^{13}\text{CH}$ features are detected with confidence, so we simply adopt ${}^{12}\text{C}/{}^{13}\text{C} = 5$ in our syntheses. Carbon is depleted during the normal course of stellar evolution, and the natal abundance in HD 222925 may have been higher by $\approx +0.46$ dex (Placco et al. 2014), yielding an initial $[\text{C}/\text{Fe}] \approx +0.26$. HD 222925

⁷ Ionized Co, the majority species, is not often analyzed in the spectra of late-type stars. Close inspection of Figure 1 reveals a relatively unblended Co II line at 3501.72 Å in HD 222925. A recent laboratory analysis of Co II $\log gf$ values by Lawler et al. (2018) did not report a $\log gf$ value for this line, because it is a weak branch from the upper level and is blended in their spectrum. The six other Co II lines with $\log gf$ values reported by Lawler et al. that are covered by our MIKE spectrum appear blended in HD 222925, and we are unable to derive Co abundances from them.

implicitly captures the covariances between element ratios, and these samples are run simultaneously with the [Fe/H] samples, so the results are self-consistent. Table 3 lists the median abundances, uncertainties, and number of lines used to derive the abundance for each species. The 16th and 84th percentiles of the distributions are roughly symmetric, so only one number is listed as the uncertainty for each abundance or ratio in Table 3.

Non-LTE corrections for Na I lines, when available from the INSPECT database (Lind et al. 2011), are reflected in the values presented in Tables 2 and 3. The average non-LTE correction for six of the Na I lines is -0.16 dex. The Na I line at 4982.81 \AA is not included in the INSPECT database, so we adopt its LTE abundance. We adopt the non-LTE correction, -0.62 dex, interpolated from the grid of Takeda et al. (2002) for the K I line at 7698.96 \AA . This correction is also reflected in the values presented in Tables 2 and 3.

The [X/Fe] ratios derived from the minority (neutral) species of Ti, V, and Mn are slightly deficient (0.10 – 0.16 dex) relative to the ratios derived from their ions. Similarly, the [Sr/Fe] ratio derived from the Sr I line at 4607.33 \AA is deficient by 0.41 dex relative to that derived from Sr II lines. Overionization is likely affecting these species (cf. Bergemann & Gehren 2008; Bergemann 2011; Hansen et al. 2013), so we favor the abundances and ratios derived from lines of their ions. The [Cu/Fe] ratio, derived from one Cu I line, likely underestimates the true value by a few tenths of a dex (Korotin et al. 2018; Roederer & Barklem 2018). Most heavy elements are detected in ionization states that represent a substantial fraction, if not a majority, of all atoms of each element. Departures from LTE are expected to be small for these species, but Pb is an exception. We derive an upper limit from one Pb I line, and Mashonkina et al. (2012) have shown that non-LTE corrections can be substantial (>0.2 dex) for Pb I lines in metal-poor dwarf and giant stars. It is possible that the upper limit we have inferred is underestimated by a few tenths of a dex in LTE.

5.1. Abundances in the Balmer Dip Region

Previous studies have shown that abundances of Ti I, Ti II, and Fe I yield abundances that are lower by ≈ 0.08 – 0.27 dex when derived from lines in the 3100 – 3700 \AA region in warm metal-poor dwarfs (Lawler et al. 2013; Wood et al. 2013; Sneden et al. 2016; Roederer et al. 2018b) and cool giants (Roederer et al. 2012). This phenomenon is referred to as the Balmer Dip effect. These studies concluded that unaccounted continuous opacity, non-LTE effects in individual metal ions or levels, and non-LTE effects in the H I $n = 2$ level cannot fully explain all observations available at present. Three-dimensional convection effects have been suggested as a possible explanation.

Nine species in our study have at least three lines in the Balmer Dip region and at least three lines at longer wavelengths, which we consider minimally sufficient to assess whether a similar effect may occur in HD 222925. Three of these species are Fe-group species (V II, Fe I, and Co I), and the other six species are heavy elements (Y II, Zr II, Gd II, Dy II, Ho II, and Er II). The differences between mean abundances derived from lines with $\lambda < 3700 \text{ \AA}$ and $\lambda > 3700 \text{ \AA}$ are not significant at the $\approx 1.2\sigma$ level. Only Zr II shows a marginally significant discrepancy, where 35 Zr II lines with $\lambda > 3700 \text{ \AA}$ yield an abundance 0.10 ± 0.04 dex higher than 16 Zr II lines at shorter

wavelengths. Roederer et al. (2018b) noted that the effect appeared muted, when it appeared at all in warmer stars. Our results support and extend that conclusion.

6. Discussion

6.1. Elements with $Z \leq 30$

We derive abundances for 18 metals with $Z \leq 30$ in HD 222925. Figure 2 illustrates the [X/Fe] ratios, where X represents a particular element. Several sets of abundance ratios from the literature are shown for comparison. We prioritize comparisons with analyses of large numbers of RHB stars in the field, which may help to minimize systematic uncertainties. Abundance ratios from the RHB star samples of Preston et al. (2006), For & Sneden (2010), Roederer et al. (2014a), and Afşar et al. (2012, 2018) are shown by dark gray crosses in Figure 2. These samples offer few stars for comparison in the metallicity range around $[\text{Fe}/\text{H}] = -1.5$, so we supplement with data from other stellar types. Abundance ratios from the dwarf and giant star samples of Bensby et al. (2014), Roederer et al. (2014a), Jacobson et al. (2015), Battistini & Bensby (2015, 2016), and Hansen et al. (2018) are shown by small gray dots in Figure 2.

Figure 2 demonstrates that the abundances of elements with $Z \leq 30$ in HD 222925 match those of other metal-poor field stars with $-2 < [\text{Fe}/\text{H}] < -1$. The α -elements O (see Section 5), Mg, Si, Ca, and Ti are enhanced relative to the Sun, with $[\alpha/\text{Fe}] \approx +0.4$. The [Na/Fe] ratio and [Al/Fe] ratio (not shown) are both slightly sub-solar in HD 222925, which matches the comparison samples (see also Andrievsky et al. 2007, 2008). The [K/Fe] ratio (not shown) is slightly super-solar, and this is also normal for stars in this metallicity range (Roederer et al. 2014a). Among the Fe-group elements, [Zn/Fe] is super-solar, [Sc/Fe] and [V/Fe] (both not shown) are slightly super-solar, [Cr/Fe], [Mn/Fe], [Co/Fe], and [Ni/Fe] are solar or slightly sub-solar, and [Cu/Fe] (not shown) is significantly sub-solar in HD 222925. All of these ratios are normal for stars in this metallicity range.

Mixing processes may affect the surface composition of C and N in evolved stars like HD 222925. The [C/Fe] ratio in HD 222925 is slightly sub-solar, and we infer its natal abundance (Section 5) to have been slightly super-solar, $[\text{C}/\text{Fe}] = +0.26$, which does not qualify as being C-enhanced. The [N/Fe] ratio in HD 222925 is slightly super-solar. Both of these ratios are normal for stars on the RHB (Gratton et al. 2000).

In summary, the agreement between the abundances in HD 222925 and the comparison samples implies that normal Type II supernovae produced most of the metals with $Z \leq 30$. There are minimal, if any, contributions from Type Ia supernovae or AGB stars. HD 222925 formed in a region where chemical evolution was dominated by massive stars that enriched the local ISM to $[\text{Fe}/\text{H}] = -1.5$ relatively quickly.

6.2. Elements with $Z \geq 38$

Figure 2 illustrates the high levels of [Sr/Fe], [Zr/Fe], [Ba/Fe], [La/Fe], and [Eu/Fe] in HD 222925. The [Sr/Fe], [Zr/Fe], and [Ba/Fe] ratios are found along the upper envelope of ratios in the comparison samples, while [La/Fe] and [Eu/Fe] are significantly higher. Such high levels of enhancement are not generally found among stars with $[\text{Fe}/\text{H}] > -2$. The high [Eu/Fe] ratio ($+1.33 \pm 0.08$) and low [Ba/Eu] ratio

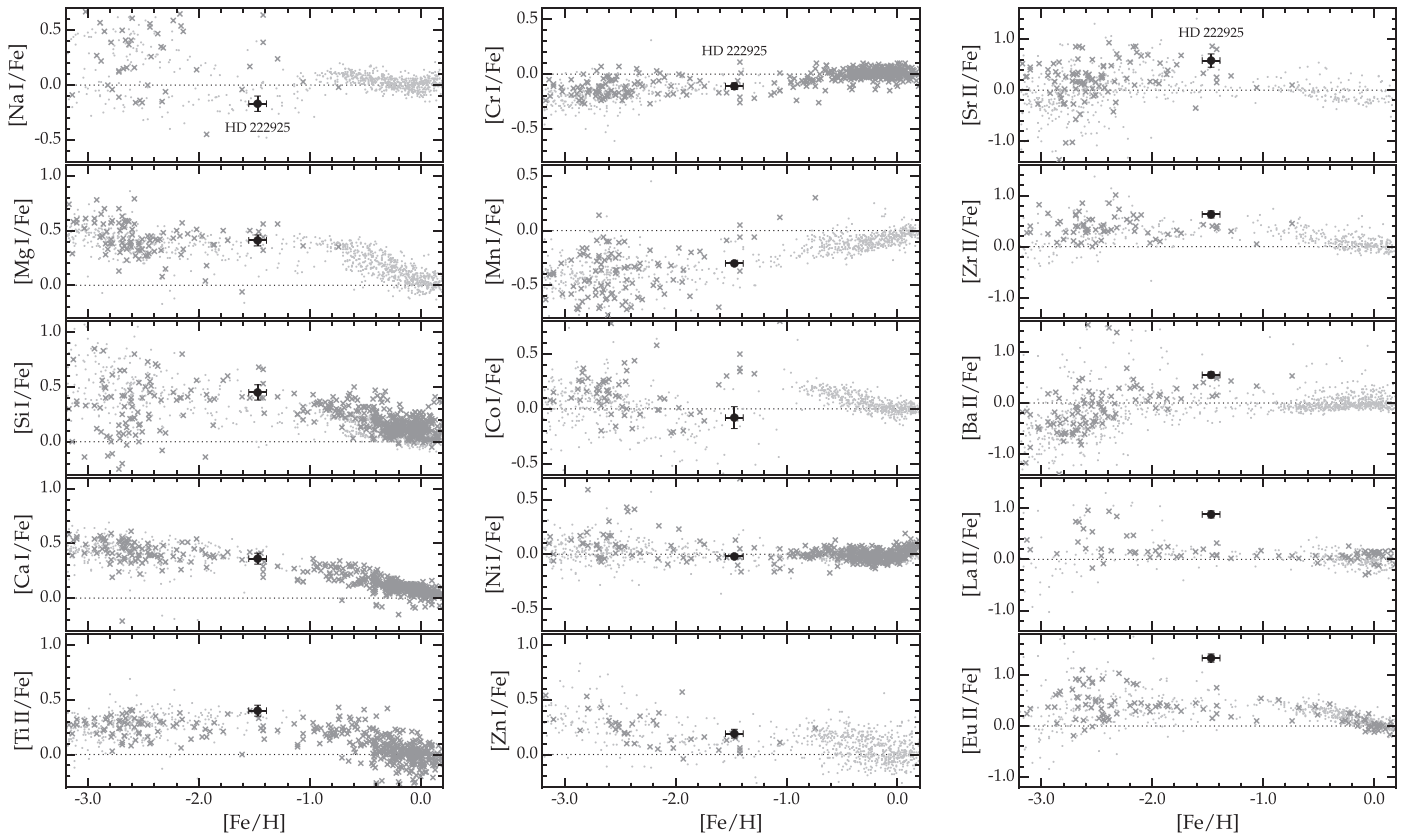


Figure 2. Comparison of abundance ratios in HD 222925 (large black circle) with other field stars. The small gray crosses represent RHB stars from Preston et al. (2006), For & Sneden (2010), Roederer et al. (2014a), and Afşar et al. (2012, 2018). The small gray dots represent dwarfs and giants from Bensby et al. (2014), Roederer et al. (2014a), Jacobson et al. (2015), Battistini & Bensby (2015, 2016), and Hansen et al. (2018). The dotted line in each panel represents the solar ratio.

(-0.78 ± 0.10) identify HD 222925 as a member of the *r*-II class of stars.

The heavy-element abundances in HD 222925 are illustrated in Figure 3. Three patterns are shown for comparison in the top panel. The pink line represents the solar *r*-process residuals (Sneden et al. 2008); this line has not been rescaled. The dark red line represents the solar *r*-process residuals when scaled down by 0.11 dex to match the Eu abundance in HD 222925. The thin blue line represents the solar *s*-process abundance pattern scaled down by 0.95 dex to match the Ba abundance in HD 222925.

The solar *r*-process residuals fit most elements well. The lanthanides ($57 \leq Z \leq 71$), plus Ba and Hf ($Z = 56$ and 72), exhibit a robust *r*-process abundance pattern. This agreement extends to the third *r*-process peak (Os and Ir; $Z = 76$ and 77). There are no significant deviations between the overall levels of Sr and Zr ($Z = 38$ and 40) and the scaled solar *r*-process residuals. The *r*-process event that enriched HD 222925 produced, at a minimum, substantial quantities of elements from $38 \leq Z \leq 90$.

It is also apparent from Figure 3 that the solar *s*-process pattern is a poor match to the HD 222925 abundances, regardless of how it is normalized. Pb lies at the end of the *s*-process nucleosynthesis chain, and it is often observed to be highly enhanced ($[\text{Pb}/\text{Fe}] > +2$) in metal-poor stars with strong *s*-process signatures (e.g., Aoki et al. 2002; Van Eck et al. 2003). Pb is often the first detectable signature of *s*-process contamination (Roederer et al. 2010a). The reasonably low limit on Pb in HD 222925, with or without non-LTE

corrections, indicates that *s*-process material is no more than minimally present in HD 222925.

6.2.1. Deviations among Some Lighter *R*-process Elements

The elements whose abundances deviate significantly from the scaled *r*-process pattern in HD 222925—Y, Rh, Pd, and Ag—deviate in a manner consistent with behavior observed in other *r*-process-enhanced stars (e.g., Johnson & Bolte 2002). Figure 4 illustrates this point. Eight *r*-process-enhanced stars are illustrated in Figure 4; they have been selected for inclusion because Ru, Rh, Pd, and Ag ($44 \leq Z \leq 47$) have been detected. Cd ($Z = 48$) has also been detected in two of them. The points in Figure 4 represent the differences between the $\log \varepsilon$ abundances and the solar *r*-process residuals, and these points have been normalized to Zr.

The Y abundances consistently deviate by ≈ -0.5 dex from the scaled solar *r*-process residuals. The downward trend relative to the scaled *r*-process residuals for $44 \leq Z \leq 47$ appears to be a distinct characteristic of the *r*-process signature. It is unclear whether this trend extends to Cd, because Cd has been detected in so few stars. The deviations for the $44 \leq Z \leq 47$ elements also become more pronounced as the $[\text{Eu}/\text{Fe}]$ (or $[\text{Zr}/\text{Fe}]$) ratios decrease, which reaffirms the conclusion of Hansen et al. (2012) that production of these elements is not always fully coupled to Zr or Eu. The similar abundance ratios among the $38 \leq Z \leq 47$ elements for the stars in the top five panels of Figure 4 indicate relatively robust production ratios among the *r*-process events that enriched these *r*-II stars.

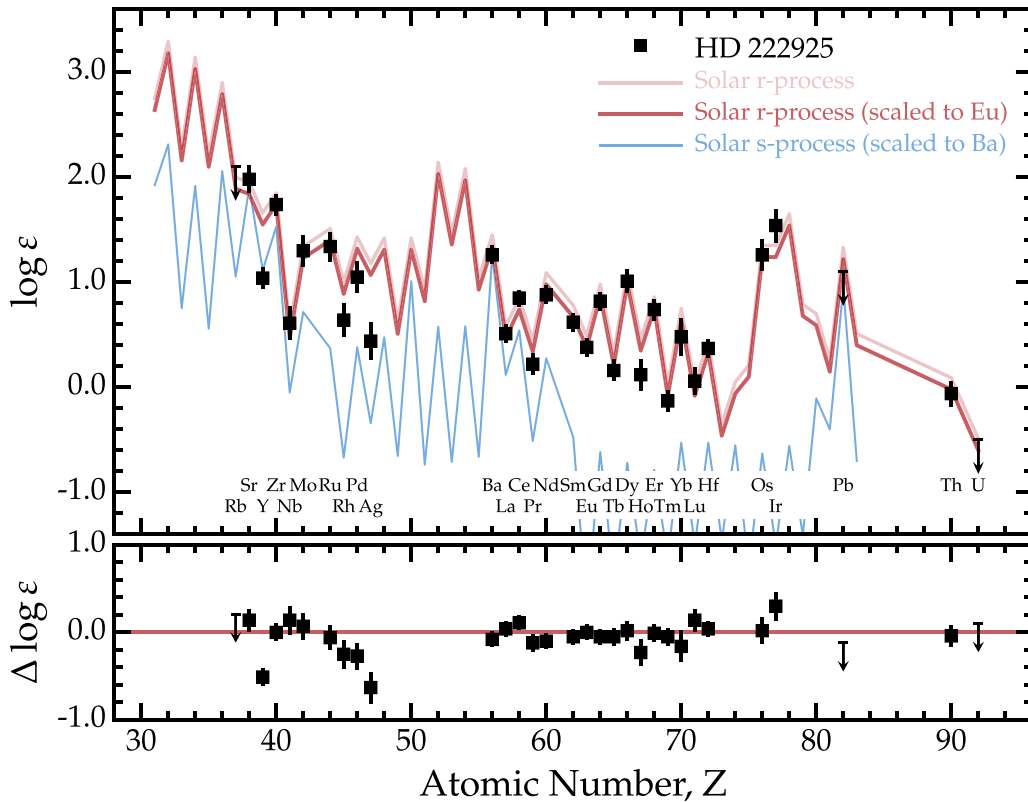


Figure 3. Top panel: comparison between the heavy-element abundances in HD 222925 and the solar r - and s -process patterns (Snedden et al. 2008). The solar r -process residual pattern (thick red line) is normalized to the Eu abundance, and the solar s -process pattern (thin blue line) is normalized to the Ba abundance. The pink line marks an unscaled version of the solar r -process residual pattern. Bottom panel: differences between the HD 222925 abundances and the scaled solar r -process residuals.

6.2.2. The Actinides

The ^{232}Th isotope is the only heavy, radioactive isotope detected in HD 222925. Five lines of Th II are detected, and all give concordant abundances. The ^{238}U isotope cannot be detected because blends comprise U II lines that might otherwise be detectable at 3550.82 Å (blended with La II), 3859.57 Å (Fe I), 4050.13 Å (La II), 4090.13 Å (Fe I), and 4241.66 Å (Zr I).

The actinide elements Th and U can only be produced by r -process nucleosynthesis, but their production is not well-understood theoretically at present. There appears to be a genuine dispersion among the $\log \varepsilon(\text{Th}/\text{Eu})$ ratios of metal-poor, r -process enhanced stars, ranging from -0.12 (2MASS J0954+5246; Holmbeck et al. 2018a) to -0.84 (DES J0335–5404; Ji & Frebel 2018). The mean $\log \varepsilon(\text{Th}/\text{Eu})$ ratio in HD 222925 lies between these extremes, -0.44 ± 0.14 . For completeness, we note that the $\log \varepsilon(\text{Th}/\text{Eu})$ ratio derived from only the Th II line at 4019.13 Å, which is often the only Th abundance indicator in other stars, is -0.61 in HD 222925; this ratio closely matches that found in other r -II stars.

The dispersion among the observed ratios is known as the “actinide boost” (Hill et al. 2002; Schatz et al. 2002). This phenomenon results in enhanced abundances of Th and U relative to levels expected based on the low metallicities (i.e., old ages) and predictions for actinide production relative to lighter, stable isotopes. Recent observations of the brightest r -process-enhanced star in Reticulum II by Ji & Frebel (2018) suggest the existence of actinide-deficient stars as well. Attempts to characterize actinide production using globular

clusters of known ages have so far been unsuccessful due to the large observational uncertainties, small number of clusters studied, and the lack of actinide-boost signatures in any cluster studied (Roederer & Thompson 2015; Roederer et al. 2016). New theoretical efforts to understand the physical nature of the actinide boost phenomenon (e.g., Holmbeck et al. 2018b) are most welcome. We thus refrain from estimating the age of HD 222925 from the radioactive decay of ^{232}Th .

6.3. The Environment of HD 222925

In this section, we consider additional kinematic and chemical information to infer possible origin scenarios for HD 222925. Roederer et al. (2018a) identified HD 222925 as a member of a group of kinematically similar r -process-enhanced stars. This group and others were identified using only the stars’ specific orbital energy and action integrals. Chemistry played no role in the group definitions, yet the $[\text{Fe}/\text{H}]$ dispersion of each group was considerably smaller than would be expected if the groups were selected at random among the r -process-enhanced stars considered. The $[\text{Fe}/\text{H}]$ dispersions of these groups are comparable to or smaller than that found among the r -process-enhanced stars in the Reticulum II dwarf galaxy. Other low-mass dwarf galaxies typically show moderately small $[\text{Fe}/\text{H}]$ dispersions (≈ 0.3 – 0.6 dex; e.g., Kirby et al. (2011b)). This line of reasoning led Roederer et al. to conclude that r -process-enhanced stars within each candidate group may share a common origin.

The two other stars that are candidates for membership in the group with HD 222925, HD 20 and J0153–3417 = HD 11582,

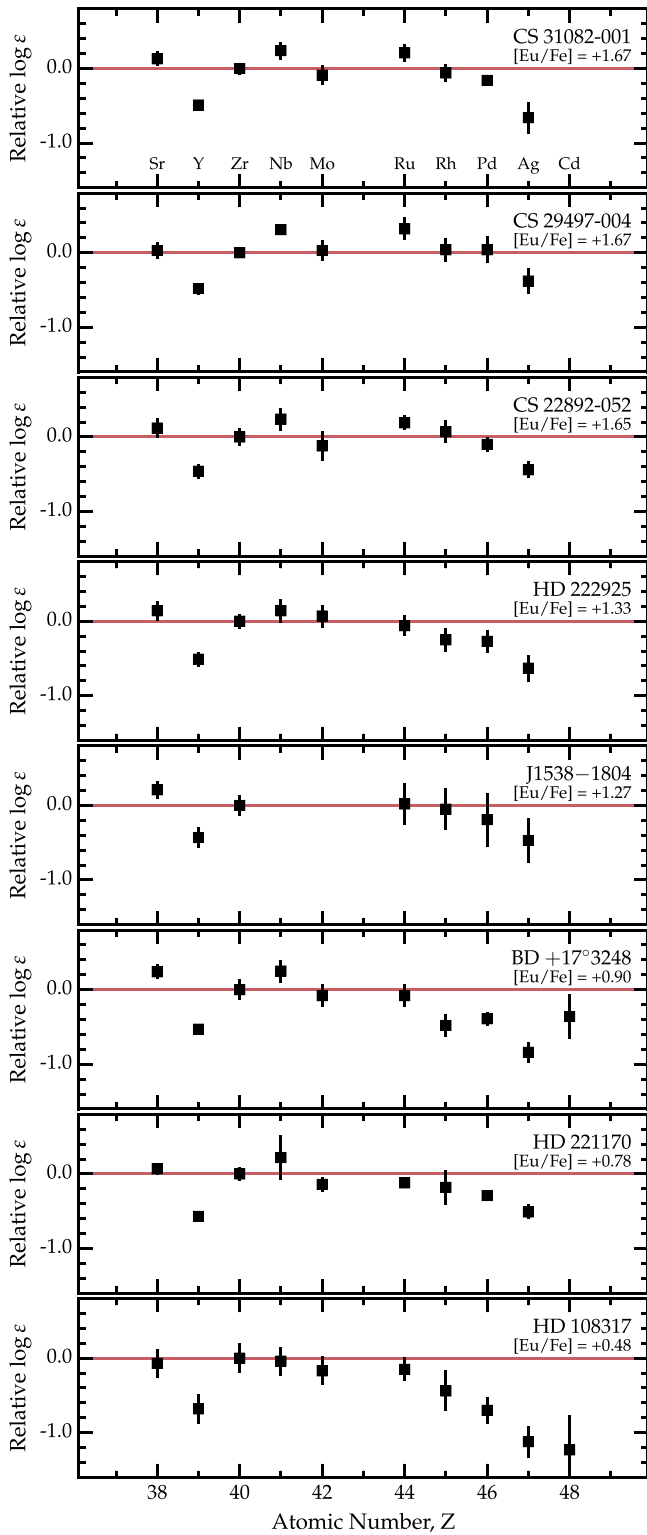


Figure 4. Differences between the $38 \leq Z \leq 48$ abundances and the solar r -process residuals (Sneden et al. 2008) for eight r -process-enhanced stars. The differences are normalized to Zr. The red line in each panel indicates perfect agreement with the r -process residuals. Data are taken from Siqueira Mello et al. (2013) for CS 31082-001, Hill et al. (2017) for CS 29497-004, Sneden et al. (2003) for CS 22892-052, this study for HD 222925, Sakari et al. (2018b) for J15383085–1804242, Cowan et al. (2002) and Roederer et al. (2010b) for BD +17°3248, Ivans et al. (2006) for HD 221170, and Roederer et al. (2012, 2014b) for HD 108317. The stars are sorted by decreasing [Eu/Fe] ratios, which are adopted from Sneden et al. (2009) or the references given above.

have similarly high [Fe/H] ratios, -1.58 and -1.50 (Barklem et al. 2005; Hansen et al. 2018). Their [Eu/H] ratios, -0.78 and -0.79 , are high, but lower than HD 222925. The stars in this group have highly eccentric, retrograde orbits that pass within ~ 1 kpc of the Galactic center and extend to ~ 15 kpc from the Galactic center. Any stellar system with such a small pericentric radius would be quickly tidally disrupted by the Milky Way, so chemical evolution in the progenitor would have been truncated as soon as it was accreted. This conclusion is consistent with our finding that the metals in HD 222925 were produced on short timescales by Type II supernovae.

The metallicity dispersion of the three stars is small and consistent with zero, like that of most globular clusters. It is unlikely, however, that the progenitor was a globular cluster. Neither HD 222925 nor the other stars in this group exhibit the light-element chemical signatures among O, Na, Mg, or Al that are commonly found among the majority of globular cluster stars (Barklem et al. 2005; Roederer et al. 2014a). Furthermore, no star is known in any globular cluster with [Eu/Fe] as enhanced as HD 222925.

Roederer et al. (2018a) instead proposed that these three stars may represent a few of the remnants from a dwarf galaxy. The dwarf galaxy luminosity–metallicity relation (Kirby et al. 2008; Walker et al. 2016) predicts a satellite progenitor with a mass or luminosity comparable to that of the Sculptor dwarf galaxy ($M_* \approx 2.3 \times 10^6 M_\odot$; McConnachie 2012). We regard this as unlikely because few known field r -process-enhanced stars have such high metallicities. Instead, we speculate that these three stars may have formed in a relatively dense clump of gas in close proximity to an r -process event in the putative progenitor satellite.

A few moderately metal-poor r -II stars are known in the low-luminosity classical dwarf galaxies Draco (Dra) (Cohen & Huang 2009) and Ursa Minor (UMi) (Shetrone et al. 2001). One of those stars, UMi COS 82 (Aoki et al. 2007b), has a metallicity ([Fe/H] = -1.42) and Eu abundance ([Eu/H] = -0.18) similar to those of HD 222925. There is a more continuous rise in [Eu/Fe] with increasing [Fe/H] in UMi (Cohen & Huang 2010), suggesting that multiple r -process events may have occurred in this system. Unlike HD 222925, which has $[\alpha/\text{Fe}] \approx +0.4$, the $[\alpha/\text{Fe}]$ ratios of UMi COS 82 and other stars with [Fe/H] ≈ -1.5 in Dra and UMi are sub-solar or only slightly super-solar (Sadakane et al. 2004; Kirby et al. 2011a). This signals the presence of Type Ia supernova ejecta, indicating that the chemical enrichment timescales in Dra and UMi were longer than in the progenitor system of HD 222925. The longer timescales may have permitted multiple r -process events to have occurred in Dra and UMi (cf. Tsujimoto et al. 2017). HD 222925 probably did not form in systems like these.

It is probable that the r -process material observed in HD 222925 was produced by a single r -process event (cf. Ji et al. 2016a; Tsujimoto et al. 2017). Following Roederer et al. (2018a), we estimate the mass of stars formed with HD 222925 using the derived [Eu/H] ratios, adopting an r -process mass yield, and making reasonable assumptions about the star formation efficiency and metal loss from the progenitor system. A neutron star merger, like that associated with the GW170817 event, could eject $\sim 0.005 M_\odot$ of r -process material at and beyond the second r -process peak (see discussion in Côté et al. 2018). Incorporating this ejecta

into $\sim 10^3$ to $10^4 M_\odot$ of stars formed after the merger would produce the observed [Eu/H] ratios, assuming a star formation efficiency of $\sim 1\%$ and no loss of r -process metals. This mass is comparable to that of the lowest-mass dwarf galaxies known today, including Reticulum II (Ji et al. 2016c) and Tucana III (Hansen et al. 2017), which are known to contain r -process-enhanced stars. There is considerable scatter among the [Eu/H] ratios of individual stars in these systems ($-1.6 \leq [\text{Eu}/\text{H}] \leq -0.3$), and the average [Eu/H] ratio of stars in a system may provide a more meaningful measure than that from any one star. Our order-of-magnitude estimate is suggestive, but of course identifying other stars with kinematic properties similar to HD 222925 would help characterize the chemical evolution and nature of this putative progenitor system.

One star with relatively high metallicity ([Fe/H] = -1.67) and r -process enhancement ([Eu/Fe] = $+0.99$; [Eu/H] = -0.68) has been found along a line of sight toward the Milky Way bulge (2MASS J18174532–3353235; Johnson et al. 2013). This star is α -enhanced, like HD 222925, and the r -process pattern of both stars closely matches that found in r -process-enhanced stars with $-3.5 \leq [\text{Fe}/\text{H}] \leq -2.0$. The existence of stars like 2MASS J18174532–3353235 and HD 222925—which are relatively metal-rich, α -enhanced, and contain large proportions of r -process elements—supports the early onset of the r -process from a single class of progenitors, without needing to invoke mixing of multiple progenitor types.

6.4. Are There Other Misclassified R -process-enhanced Stars?

We noted in Section 1 that Houk & Cowley (1975) classified HD 222925 as being a chemically peculiar “Sr Eu” star. Are there other r -process-enhanced stars in this catalog or subsequent ones (Houk 1978, 1982; Houk & Smith-Moore 1988; Houk & Swift 1999) that have been overlooked? Houk and colleagues classified Ap (“peculiar A”) stars by the relative strengths of several metal lines, including Cr II ($\lambda 4111$, $\lambda 4171$), Sr II ($\lambda 4077$, $\lambda 4216$), and Eu II ($\lambda 4128$ – 30). HD 222925 was not designated with “Cr,” which indicates its metal lines are relatively weak. These catalogs list 36 stars designated with “Eu” but not “Cr.” Eleven of these stars have been identified as α^2 CVn variables (Bernhard et al. 2015), which have strong surface magnetic fields that stratify metals in the atmosphere. One is a confirmed δ Scv variable (Martinez 2002). Another 22 of these stars have T_{eff} estimates (McDonald et al. 2012; I.U.R., unpublished) between ~ 6500 and 9500 K that suggest they are not late-type metal-poor stars. Several of these stars are also well-studied chemically peculiar standards, often exhibiting Zeeman splitting of metal absorption lines (e.g., Freyhammer et al. 2008). The only star among the 36 that is not described by any of these characteristics is HD 222925. We conclude that it is unlikely that other stars like HD 222925 have been overlooked based on their initial classification in the catalogs by Houk and colleagues.

7. Conclusions

We present a detailed analysis of the stellar parameters and abundances of the bright, metal-poor star HD 222925. This star is a field equivalent of the He core-burning RHB stars found in metal-poor globular clusters. HD 222925 is the brightest r -II star known ($V = 9.02$), one of the warmest r -II stars known ($T_{\text{eff}} = 5636$ K), the most metal-rich r -II star known

([Fe/H] = -1.47), and contains the highest abundance of r -process elements ([Eu/H] = -0.14) among r -process-enhanced stars.

HD 222925 shows no evidence of binarity, and it is not enhanced in carbon. HD 222925 is α -enhanced, with [(O, Mg, Si, Ca, Ti)/Fe] $\approx +0.4$, and the abundance ratios among elements with $Z \leq 30$ are consistent with other metal-poor field stars. The heavy elements are highly enhanced in HD 222925, perhaps best exemplified by [Eu/Fe] = $+1.33$. The abundances of elements with $Z \geq 38$ closely match the scaled solar r -process residuals, with no evidence for s -process contamination. Deviations from the solar r -process pattern for Y, Ru, Rh, Pd, and Ag ($Z = 39, 44$ – 47) match those found in other r -process-enhanced stars. HD 222925 does not exhibit a strong actinide boost, but the $\log \varepsilon(\text{Th}/\text{Eu})$ ratio, -0.44 , is intermediate between stars with and without the actinide boost.

HD 222925 is a member of a group of r -process-enhanced stars with similar kinematics (Roederer et al. 2018a). If we assume that the r -process material in HD 222925 was produced by a single, high-yield nucleosynthesis event, like a neutron star merger, we conclude that the progenitor system had a stellar mass $\sim 10^3$ – $10^4 M_\odot$, comparable to the surviving population of ultra-faint dwarf galaxies. This conclusion is consistent with our assertion that the metals with $Z \leq 30$ in HD 222925 were produced by Type II supernovae with minimal contributions from Type Ia supernovae or AGB stars, as is typical for the surviving population of ultra-faint dwarf galaxies (e.g., Frebel et al. 2014; Ji et al. 2016b). The existence of relatively metal-rich stars, such as HD 222925, with r -process abundance signatures that are excellent matches to r -II stars with $-3.5 \leq [\text{Fe}/\text{H}] \leq -2.0$, supports the early onset of the r -process from a single class of progenitors, without needing to invoke mixing of multiple progenitor types.

We thank the referee for a prompt and constructive report. I.U.R., V.M.P., T.C.B., R.E., and A.F. acknowledge financial support from grant PHY 14-30152 (Physics Frontier Center/JINA-CEE) awarded by the U.S. National Science Foundation (NSF). I.U.R. acknowledges support from NSF grants AST-1613536 and AST-1815403. C.M.S. acknowledges funding from the Kenilworth Fund of the New York Community Trust. A.F. acknowledges support from NSF grant AST-1716251. This research has made use of NASA’s Astrophysics Data System Bibliographic Services; the arXiv pre-print server operated by Cornell University; the SIMBAD and VizieR databases hosted by the Strasbourg Astronomical Data Center; the ASD hosted by NIST; and Image Reduction and Analysis Facility (IRAF) software packages distributed by the National Optical Astronomy Observatories, which are operated by AURA, under cooperative agreement with the NSF. This work has also made use of data from the European Space Agency (ESA) mission *Gaia* (<http://www.cosmos.esa.int/gaia>), processed by the *Gaia* Data Processing and Analysis Consortium (DPAC, <http://www.cosmos.esa.int/web/gaia/dpac/consortium>). Funding for the DPAC has been provided by national institutions, particularly the institutions participating in the *Gaia* Multilateral Agreement.

Facility: Magellan (MIKE).

Software: IRAF (Tody 1993), matplotlib (Hunter 2007), MOOG (Snedden 1973), numpy (van der Walt et al. 2011), R (R Core Team 2013), scipy (Jones et al. 2001).

ORCID iDs

Ian U. Roederer  <https://orcid.org/0000-0001-5107-8930>
 Charli M. Sakari  <https://orcid.org/0000-0002-5095-4000>
 Vinicius M. Placco  <https://orcid.org/0000-0003-4479-1265>
 Timothy C. Beers  <https://orcid.org/0000-0003-4573-6233>
 Rana Ezzeddine  <https://orcid.org/0000-0002-8504-8470>
 Anna Frebel  <https://orcid.org/0000-0002-2139-7145>
 Terese T. Hansen  <https://orcid.org/0000-0001-6154-8983>

References

- Abbott, B. P., Abbott, R., Abbott, T. D., et al. 2017a, *PhRvL*, **119**, 161101
 Abbott, B. P., Abbott, R., Abbott, T. D., et al. 2017b, *ApJL*, **848**, L12
 Afşar, M., Bozkurt, Z., Böcek Topcu, G., et al. 2018, *AJ*, **155**, 240
 Afşar, M., Sneden, C., & For, B.-Q. 2012, *AJ*, **144**, 20
 Aldenius, M., Lundberg, H., & Blackwell-Whitehead, R. 2009, *A&A*, **502**, 989
 Alonso, A., Arribas, S., & Martínez-Roger, C. 1999, *A&AS*, **140**, 261
 Andrievsky, S. M., Spite, M., Korotin, S. A., et al. 2007, *A&A*, **464**, 1081
 Andrievsky, S. M., Spite, M., Korotin, S. A., et al. 2008, *A&A*, **481**, 481
 Aoki, W., Beers, T. C., Christlieb, N., et al. 2007a, *ApJ*, **655**, 492
 Aoki, W., Honda, S., Sadakane, K., & Arimoto, N. 2007b, *PASJ*, **59**, L15
 Aoki, W., Ryan, S. G., Norris, J. E., et al. 2002, *ApJ*, **580**, 1149
 Asplund, M., Grevesse, N., Sauval, A. J., & Scott, P. 2009, *ARA&A*, **47**, 481
 Bailer-Jones, C. A. L., Rybizki, J., Fouesneau, M., Mantelet, G., & Andrae, R. 2018, *AJ*, **156**, 58
 Barklem, P. S., & Asplund-Johansson, J. 2005, *A&A*, **435**, 373
 Barklem, P. S., Christlieb, N., Beers, T. C., et al. 2005, *A&A*, **439**, 129
 Barklem, P. S., Piskunov, N., & O'Mara, B. J. 2000, *A&A*, **355**, L5
 Battistini, C., & Bensby, T. 2015, *A&A*, **577**, A9
 Battistini, C., & Bensby, T. 2016, *A&A*, **586**, A49
 Beers, T. C., & Christlieb, N. 2005, *ARA&A*, **43**, 531
 Beers, T. C., Norris, J. E., Placco, V. M., et al. 2014, *ApJ*, **794**, 58
 Beers, T. C., Preston, G. W., & Shectman, S. A. 1992, *AJ*, **103**, 1987
 Belmonte, M. T., Pickering, J. C., Ruffoni, M. P., et al. 2017, *ApJ*, **848**, 125
 Beniamini, P., Hotokezaka, K., & Piran, T. 2016, *ApJ*, **832**, 149
 Bensby, T., Feltzing, S., & Oey, M. S. 2014, *A&A*, **562**, A71
 Bergemann, M. 2011, *MNRAS*, **413**, 2184
 Bergemann, M., & Gehren, T. 2008, *A&A*, **492**, 823
 Bergemann, M., Lind, K., Collet, R., Magic, Z., & Asplund, M. 2012, *MNRAS*, **427**, 27
 Bernhard, K., Hümmerich, S., Otero, S., & Paunzen, E. 2015, *A&A*, **581**, A138
 Bernstein, R., Shectman, S. A., Gunnels, S. M., Mochnacki, S., & Athey, A. E. 2003, *Proc. SPIE*, **4841**, 1694
 Biémont, E., Garnir, H. P., Palmeri, P., Li, Z. S., & Svanberg, S. 2000, *MNRAS*, **312**, 116
 Biémont, É., Blagoev, K., Engström, L., et al. 2011, *MNRAS*, **414**, 3350
 Cain, M., Frebel, A., Gull, M., et al. 2018, *ApJ*, **864**, 43
 Casagrande, L., Portinari, L., Glass, I. S., et al. 2014, *MNRAS*, **439**, 2060
 Casagrande, L., Ramírez, I., Meléndez, J., Bessell, M., & Asplund, M. 2010, *A&A*, **512**, A54
 Casagrande, L., & VandenBerg, D. A. 2014, *MNRAS*, **444**, 392
 Castellì, F., & Kurucz, R. L. 2004, arXiv:astro-ph/0405087
 Cayrel, R. 1988, in IAU Symp. 132, The Impact of Very High S/N Spectroscopy on Stellar Physics, ed. G. Cayrel de Strobel & M. Spite (Dordrecht: Kluwer), **345**
 Cayrel, R., Depagne, E., Spite, M., et al. 2004, *A&A*, **416**, 1117
 Cohen, J. G., Christlieb, N., McWilliam, A., et al. 2008, *ApJ*, **672**, 320
 Cohen, J. G., & Huang, W. 2009, *ApJ*, **701**, 1053
 Cohen, J. G., & Huang, W. 2010, *ApJ*, **719**, 931
 Côté, B., Fryer, C. L., Belczynski, K., et al. 2018, *ApJ*, **855**, 99
 Cowan, J. J., Sneden, C., Beers, T. C., et al. 2005, *ApJ*, **627**, 238
 Cowan, J. J., Sneden, C., Burles, S., et al. 2002, *ApJ*, **572**, 861
 Cowperthwaite, P. S., Berger, E., Villar, V. A., et al. 2017, *ApJL*, **848**, L17
 Cutri, R. M., Skrutskie, M. F., van Dyk, S., et al. 2003, *yCat*, **2246**
 Den Hartog, E. A., Lawler, J. E., Sneden, C., & Cowan, J. J. 2003, *ApJS*, **148**, 543
 Den Hartog, E. A., Lawler, J. E., Sneden, C., & Cowan, J. J. 2006, *ApJS*, **167**, 292
 Den Hartog, E. A., Lawler, J. E., Sobeck, J. S., Sneden, C., & Cowan, J. J. 2011, *ApJS*, **194**, 35
 Den Hartog, E. A., Ruffoni, M. P., Lawler, J. E., et al. 2014, *ApJS*, **215**, 23
 Drout, M. R., Piro, A. L., Shappee, B. J., et al. 2017, *Sci*, **358**, 1570
 Duquette, D. W., & Lawler, J. E. 1985, *JOSAB*, **2**, 1948
 Ezzeddine, R., Frebel, A., & Plez, B. 2017, *ApJ*, **847**, 142
 For, B.-Q., & Sneden, C. 2010, *AJ*, **140**, 1694
 Frebel, A. 2018, *ARNPS*, **68**, 237
 Frebel, A., Collet, R., Eriksson, K., Christlieb, N., & Aoki, W. 2008, *ApJ*, **684**, 588
 Frebel, A., Simon, J. D., & Kirby, E. N. 2014, *ApJ*, **786**, 74
 Freyhammer, L. M., Elkin, V. G., Kurtz, D. W., Mathys, G., & Martínez, P. 2008, *MNRAS*, **389**, 441
 Gratton, R. G., Sneden, C., Carretta, E., & Bragaglia, A. 2000, *A&A*, **354**, 169
 Gull, M., Frebel, A., Cain, M. G., et al. 2018, *ApJ*, **862**, 174
 Hansen, C. J., Bergemann, M., Cescutti, G., et al. 2013, *A&A*, **551**, A57
 Hansen, C. J., Primas, F., Hartman, H., et al. 2012, *A&A*, **545**, A31
 Hansen, T. T., Holmbeck, E. M., Beers, T. C., et al. 2018, *ApJ*, **858**, 92
 Hansen, T. T., Simon, J. D., Marshall, J. L., et al. 2017, *ApJ*, **838**, 44
 Hill, V., Christlieb, N., Beers, T. C., et al. 2017, *A&A*, **607**, A91
 Hill, V., Plez, B., Cayrel, R., et al. 2002, *A&A*, **387**, 560
 Holmbeck, E. M., Beers, T. C., Roederer, I. U., et al. 2018a, *ApJL*, **859**, L24
 Holmbeck, E. M., Surman, R., Sprouse, T. M., et al. 2018b, arXiv:1807.06662
 Horowitz, C. J., Arcones, A., Côté, B., et al. 2018, arXiv:1805.04637
 Houk, N. 1978, Michigan Catalogue of Two-dimensional Spectral Types for the HD Stars (Ann Arbor, MI: Univ. Michigan Press)
 Houk, N. 1982, Michigan Catalogue of Two-dimensional Spectral Types for the HD Stars, Vol. 3 (Ann Arbor, MI: Univ. Michigan Press)
 Houk, N., & Cowley, A. P. 1975, University of Michigan Catalogue of Two-dimensional Spectral Types for the HD Stars, Vol. 1 (Ann Arbor, MI: Univ. Michigan Press)
 Houk, N., & Smith-Moore, M. 1988, Michigan Catalogue of Two-dimensional Spectral Types for the HD Stars, Vol. 4 (Ann Arbor, MI: Univ. Michigan Press)
 Houk, N., & Swift, C. 1999, Michigan Catalogue of Two-dimensional Spectral Types for the HD Stars, Vol. 5 (Ann Arbor, MI: Univ. Michigan Press)
 Hunter, J. D. 2007, *CSE*, **9**, 90
 Ivans, I. I., Simmerer, J., Sneden, C., et al. 2006, *ApJ*, **645**, 613
 Ivarsson, S., Litzén, U., & Wahlgren, G. M. 2001, *PhysS*, **64**, 455
 Jacobson, H. R., Keller, S., Frebel, A., et al. 2015, *ApJ*, **807**, 171
 Ji, A. P., & Frebel, A. 2018, *ApJ*, **856**, 138
 Ji, A. P., Frebel, A., Chiti, A., & Simon, J. D. 2016a, *Natur*, **531**, 610
 Ji, A. P., Frebel, A., Ezzeddine, R., & Casey, A. R. 2016b, *ApJL*, **832**, L3
 Ji, A. P., Frebel, A., Simon, J. D., & Chiti, A. 2016c, *ApJ*, **830**, 93
 Johnson, C. I., McWilliam, A., & Rich, R. M. 2013, *ApJL*, **775**, L27
 Johnson, J. A., & Bolte, M. 2002, *ApJ*, **579**, 616
 Jones, E., Oliphant, T., Peterson, P., et al. 2001, SciPy: Open Source Scientific Tools for Python, <http://www.scipy.org/>
 Kasen, D., Metzger, B., Barnes, J., Quataert, E., & Ramirez-Ruiz, E. 2017, *Natur*, **551**, 80
 Katz, D., Sartoretti, P., Cropper, M., et al. 2018, *A&A*, submitted (arXiv:1804.09372)
 Kelson, D. D. 2003, *PASP*, **115**, 688
 Kelson, D. D., Illingworth, G. D., van Dokkum, P. G., & Franx, M. 2000, *ApJ*, **531**, 159
 Kirby, E. N., Cohen, J. G., Smith, G. H., et al. 2011a, *ApJ*, **727**, 79
 Kirby, E. N., Lanfranchi, G. A., Simon, J. D., Cohen, J. G., & Guhathakurta, P. 2011b, *ApJ*, **727**, 78
 Kirby, E. N., Simon, J. D., Geha, M., Guhathakurta, P., & Frebel, A. 2008, *ApJL*, **685**, L43
 Kordopatis, G., Gilmore, G., Steinmetz, M., et al. 2013, *AJ*, **146**, 134
 Korotin, S. A., Andrievsky, S. M., & Zhukova, A. V. 2018, *MNRAS*, **480**, 965
 Kramida, A., Ralchenko, Y., Reader, J., & NIST ASD Team 2018, NIST Atomic Spectra Database (ver. 5.5.6) (Gaithersburg, MD: National Institute Standards and Technology), <https://physics.nist.gov/asd>
 Kunder, A., Kordopatis, G., Steinmetz, M., et al. 2017, *AJ*, **153**, 75
 Kurucz, R. L., & Bell, B. 1995, Atomic Line List (Cambridge, MA: Smithsonian Astrophysical Observatory)
 Lawler, J. E., Bonvallet, G., & Sneden, C. 2001a, *ApJ*, **556**, 452
 Lawler, J. E., & Dakin, J. T. 1989, *JOSAB*, **6**, 1457
 Lawler, J. E., den Hartog, E. A., Labby, Z. E., et al. 2007, *ApJS*, **169**, 120
 Lawler, J. E., Den Hartog, E. A., Sneden, C., & Cowan, J. J. 2006, *ApJS*, **162**, 227
 Lawler, J. E., Feigenson, T., Sneden, C., Cowan, J. J., & Nave, G. 2018, *ApJS*, in press (arXiv:1806.00581)
 Lawler, J. E., Guzman, A., Wood, M. P., Sneden, C., & Cowan, J. J. 2013, *ApJS*, **205**, 11
 Lawler, J. E., Sneden, C., & Cowan, J. J. 2004, *ApJ*, **604**, 850
 Lawler, J. E., Sneden, C., Cowan, J. J., et al. 2008, *ApJS*, **178**, 71
 Lawler, J. E., Sneden, C., & Cowan, J. J. 2015, *ApJS*, **220**, 13

- Lawler, J. E., Sneden, C., Cowan, J. J., Ivans, I. I., & Den Hartog, E. A. 2009, *ApJS*, **182**, 51
- Lawler, J. E., Sneden, C., Nave, G., et al. 2017, *ApJS*, **228**, 10
- Lawler, J. E., Wickliffe, M. E., Cowley, C. R., & Sneden, C. 2001b, *ApJS*, **137**, 341
- Lawler, J. E., Wickliffe, M. E., den Hartog, E. A., & Sneden, C. 2001c, *ApJ*, **563**, 1075
- Lawler, J. E., Wood, M. P., Den Hartog, E. A., et al. 2014, *ApJS*, **215**, 20
- Lawler, J. E., Wyart, J.-F., & Blaise, J. 2001d, *ApJS*, **137**, 351
- Li, R., Chatelain, R., Holt, R. A., et al. 2007, *PhyS*, **76**, 577
- Lind, K., Asplund, M., Barklem, P. S., & Belyaev, A. K. 2011, *A&A*, **528**, A103
- Lind, K., Bergemann, M., & Asplund, M. 2012, *MNRAS*, **427**, 50
- Lindgren, L., Hernandez, J., Bombrun, A., et al. 2018, *A&A*, **616**, A2
- Liu, C., Deng, L.-C., Carlin, J. L., et al. 2014, *ApJ*, **790**, 110
- Ljung, G., Nilsson, H., Asplund, M., & Johansson, S. 2006, *A&A*, **456**, 1181
- Martinez, P. 2002, *Obs*, **122**, 359
- Mashonkina, L., Ryabtsev, A., & Frebel, A. 2012, *A&A*, **540**, A98
- McCall, M. L. 2004, *AJ*, **128**, 2144
- McConnachie, A. W. 2012, *AJ*, **144**, 4
- McDonald, I., Zijlstra, A. A., & Boyer, M. L. 2012, *MNRAS*, **427**, 343
- McWilliam, A. 1998, *AJ*, **115**, 1640
- Morton, D. C. 2000, *ApJS*, **130**, 403
- Navarrete, C., Chanamé, J., Ramírez, I., et al. 2015, *ApJ*, **808**, 103
- Nilsson, H., & Ivarsson, S. 2008, *A&A*, **492**, 609
- Nilsson, H., Ivarsson, S., Johansson, S., & Lundberg, H. 2002a, *A&A*, **381**, 1090
- Nilsson, H., Zhang, Z. G., Lundberg, H., Johansson, S., & Nordström, B. 2002b, *A&A*, **382**, 368
- Norris, J., Bessell, M. S., & Pickles, A. J. 1985, *ApJS*, **58**, 463
- O'Brian, T. R., Wickliffe, M. E., Lawler, J. E., Whaling, W., & Brault, J. W. 1991, *JOSAB*, **8**, 1185
- Pehlivan Rhodin, A., Hartman, H., Nilsson, H., & Jönsson, P. 2017, *A&A*, **598**, A102
- Placco, V. M., Frebel, A., Beers, T. C., & Stancliffe, R. J. 2014, *ApJ*, **797**, 21
- Placco, V. M., Holmbeck, E. M., Frebel, A., et al. 2017, *ApJ*, **844**, 18
- Preston, G. W., Sneden, C., Thompson, I. B., Shectman, S. A., & Burley, G. S. 2006, *AJ*, **132**, 85
- Qian, Y.-Z., & Wasserburg, G. J. 2007, *PhR*, **442**, 237
- Quinet, P., Palmeri, P., Biémont, É., et al. 2006, *A&A*, **448**, 1207
- Ramírez, I., Allende Prieto, C., & Lambert, D. L. 2007, *A&A*, **465**, 271
- Ramírez, I., & Meléndez, J. 2005, *ApJ*, **626**, 465
- R Core Team, 2013, R: A Language and Environment for Statistical Computing (Vienna: R Foundation for Statistical Computing)
- Roederer, I. U., & Barklem, P. S. 2018, *ApJ*, **857**, 2
- Roederer, I. U., Cowan, J. J., Karakas, A. I., et al. 2010a, *ApJ*, **724**, 975
- Roederer, I. U., Hattori, K., & Valluri, M. 2018a, *AJ*, in press (arXiv: 1808.09467)
- Roederer, I. U., & Lawler, J. E. 2012, *ApJ*, **750**, 76
- Roederer, I. U., Lawler, J. E., Sneden, C., et al. 2008, *ApJ*, **675**, 723
- Roederer, I. U., Lawler, J. E., Sobek, J. S., et al. 2012, *ApJS*, **203**, 27
- Roederer, I. U., Mateo, M., Bailey, J. I., et al. 2016, *MNRAS*, **455**, 2417
- Roederer, I. U., Preston, G. W., Thompson, I. B., et al. 2014a, *AJ*, **147**, 136
- Roederer, I. U., Schatz, H., Lawler, J. E., et al. 2014b, *ApJ*, **791**, 32
- Roederer, I. U., Sneden, C., Lawler, J. E., et al. 2018b, *ApJ*, **860**, 125
- Roederer, I. U., Sneden, C., Lawler, J. E., & Cowan, J. J. 2010b, *ApJL*, **714**, L123
- Roederer, I. U., & Thompson, I. B. 2015, *MNRAS*, **449**, 3889
- Ruffoni, M. P., Den Hartog, E. A., Lawler, J. E., et al. 2014, *MNRAS*, **441**, 3127
- Sadakane, K., Arimoto, N., Ikuta, C., et al. 2004, *PASJ*, **56**, 1041
- Sakari, C. M., Placco, V. M., Farrell, E. M., et al. 2018a, *ApJ*, submitted
- Sakari, C. M., Placco, V. M., Hansen, T., et al. 2018b, *ApJL*, **854**, L20
- Schatz, H., Toenjes, R., Pfeiffer, B., et al. 2002, *ApJ*, **579**, 626
- Schlafly, E. F., & Finkbeiner, D. P. 2011, *ApJ*, **737**, 103
- Schlaufman, K. C., & Casey, A. R. 2014, *ApJ*, **797**, 13
- Shetrone, M. D., Côté, P., & Sargent, W. L. W. 2001, *ApJ*, **548**, 592
- Siqueira Mello, C., Spite, M., Barbuy, B., et al. 2013, *A&A*, **550**, A122
- Smith, V. V., Lambert, D. L., & Nissen, P. E. 1998, *ApJ*, **506**, 405
- Sneden, C., Cowan, J. J., & Gallino, R. 2008, *ARA&A*, **46**, 241
- Sneden, C., Cowan, J. J., Kobayashi, C., et al. 2016, *ApJ*, **817**, 53
- Sneden, C., Cowan, J. J., Lawler, J. E., et al. 2003, *ApJ*, **591**, 936
- Sneden, C., Lawler, J. E., Cowan, J. J., Ivans, I. I., & Den Hartog, E. A. 2009, *ApJS*, **182**, 80
- Sneden, C., Preston, G. W., McWilliam, A., & Searle, L. 1994, *ApJL*, **431**, L27
- Sneden, C. A. 1973, PhD thesis, Univ. Texas
- Sobek, J. S., Kraft, R. P., Sneden, C., et al. 2011, *AJ*, **141**, 175
- Sobek, J. S., Lawler, J. E., & Sneden, C. 2007, *ApJ*, **667**, 1267
- Takeda, Y., Zhao, G., Chen, Y.-Q., Qiu, H.-M., & Takada-Hidai, M. 2002, *PASJ*, **54**, 275
- Tanvir, N. R., Levan, A. J., González-Fernández, C., et al. 2017, *ApJL*, **848**, L27
- Thielemann, F.-K., Eichler, M., Panov, I. V., & Wehmeyer, B. 2017, *ARNPS*, **67**, 253
- Tody, D. 1993, in ASP Conf. Ser. 52, Astronomical Data Analysis Software and Systems II, ed. R. J. Hanisch, R. J. V. Brissenden, & J. Barnes (San Francisco, CA: ASP), 173
- Tsujimoto, T., Matsuno, T., Aoki, W., Ishigaki, M. N., & Shigezumi, T. 2017, *ApJL*, **850**, L12
- Unsold, A. 1955, Physik der Sternatmosphären besonderer Berücksichtigung der Sonne (Berlin: Springer)
- van der Walt, S., Colbert, S. C., & Varoquaux, G. 2011, *CSE*, **13**, 22
- Van Eck, S., Goriely, S., Jorissen, A., & Plez, B. 2003, *A&A*, **404**, 291
- Walker, M. G., Mateo, M., Olszewski, E. W., et al. 2016, *ApJ*, **819**, 53
- Wickliffe, M. E., & Lawler, J. E. 1997, *JOSAB*, **14**, 737
- Wickliffe, M. E., Lawler, J. E., & Nave, G. 2000, *JQSRT*, **66**, 363
- Wickliffe, M. E., Salih, S., & Lawler, J. E. 1994, *JQSRT*, **51**, 545
- Wood, M. P., Lawler, J. E., Den Hartog, E. A., Sneden, C., & Cowan, J. J. 2014a, *ApJS*, **214**, 18
- Wood, M. P., Lawler, J. E., Sneden, C., & Cowan, J. J. 2013, *ApJS*, **208**, 27
- Wood, M. P., Lawler, J. E., Sneden, C., & Cowan, J. J. 2014b, *ApJS*, **211**, 20
- Xu, H. L., Svanberg, S., Quinet, P., Palmeri, P., & Biémont, É. 2007, *JQSRT*, **104**, 52